Activation of feedforward wiring in adult hippocampal neurons by the basic-helix-loop-helix transcription factor Ascl4

Luo, Wenshu ; Egger, Matteo ; Cruz-Ochoa, Natalia ; Tse, Alice ; Maloveczky, Gyula ; Tamás, Bálint ; Lukacsovich, David ; Seng, Charlotte ; Amrein, Irmgard ; Lukacsovich, Tamás ; Wolfer, David ; Földy, Csaba

DOI: https://doi.org/10.1093/pnasnexus/pgae174

PNAS Nexus, 2024, 3, pgae174
https://doi.org/10.1093/pnasnexus/pgae174
Advance access publication 3 May 2024
Research Report

Activation of feedforward wiring in adult hippocampal neurons by the basic-helix-loop-helix transcription factor Ascl4

Wenshu Luo[a], Matteo Egger[a,b], Natalia Cruz-Ochoa[a,b], Alice Tse[a], Gyula Maloveczky[a], Bálint Tamás[a], David Lukacsovich[a], Charlotte Seng[a], Irmgard Amrein[c], Tamás Lukacsovich[a], David Wolfer[c,d] and Csaba Földy[a,b,*]

[a]Laboratory of Neural Connectivity, Brain Research Institute, Faculties of Medicine and Science, University of Zürich, Zürich 8057, Switzerland
[b]Adaptive Brain Circuits in Development and Learning (AdaBD), University Research Priority Program (URPP), University of Zürich, Zürich 8057, Switzerland
[c]Institute of Anatomy, Faculty of Medicine, University of Zürich, Zürich 8057, Switzerland
[d]Institute of Human Movement Sciences and Sport, D-HEST, ETH Zürich, Zürich 8057, Switzerland
*To whom correspondence should be addressed: Email: foldy@hifo.uzh.ch
Edited By: Eric Klann

Abstract

Although evidence indicates that the adult brain retains a considerable capacity for circuit formation, adult wiring has not been broadly considered and remains poorly understood. In this study, we investigate wiring activation in adult neurons. We show that the basic-helix-loop-helix transcription factor Ascl4 can induce wiring in different types of hippocampal neurons of adult mice. The new axons are mainly feedforward and reconfigure synaptic weights in the circuit. Mice with the Ascl4-induced circuits do not display signs of pathology and solve spatial problems equally well as controls. Our results demonstrate reprogrammed connectivity by a single transcriptional factor and provide insights into the regulation of brain wiring in adults.

Keywords: adult wiring, bHLH, Ascl4, axon growth, circuit formation

Significance Statement

In contrast to developmental circuit formation, the regulation of brain wiring across the lifespan is much less understood. Understanding the molecular bases of adult wiring could provide fundamental insights into the maintenance of brain circuits and facilitate the development of new approaches for circuit therapy and repair. In this study, we show that the transcription factor Ascl4 is capable of inducing axonal wiring in different types of adult neurons.

Introduction

Studies on adult-born neurons, circadian and mating behaviors, cell reprogramming and grafting, and neurological disorders have demonstrated pronounced wiring in the adult brain (1). While adult wiring remains comparably less understood than developmental wiring, basic-helix-loop-helix (bHLH) transcription factors (TFs) have been implicated in certain forms of adult wiring. Specifically, the overexpression of Id2, which is an inhibitor of bHLH TFs (2–5), has been shown to facilitate axon regeneration in injured neurons (6–8) and induce wiring in cultured (9) and naive adult neurons (10). These findings suggest that at least some bHLH TFs suppress wiring in adults, and Id2 induces wiring by neutralizing this suppression. Although other observations suggest that bHLH TFs themselves (as opposed to their inhibition) can also promote adult wiring, for example, after cell reprogramming (1), bHLH TF–induced wiring activation in fully differentiated adult neurons has not been demonstrated yet.

The epilepsy-associated hippocampal mossy fiber sprouting (MFS) is a robust model to gain insights into adult wiring. During MFS, such as that induced by kainic acid (KA), dentate granule cells (GCs) form three fundamentally different circuit motifs by growing new axons into the (i) ipsilateral dentate layers (feedback or recurrent wiring) (10–13), (ii) ipsilateral hilus and possibly CA3 area (feedforward wiring) (11), and (iii) contralateral hippocampus (commissural wiring) (14). The feedback motif is atypical in the sense that, with the exception of the temporal pole of the hippocampus, it does not exist in the naive brain (15), whereas the feedforward and commissural motifs are typical, although naive commissural GC projections are infrequent (14). Previously, we showed that feedback, but neither

Competing Interest: The authors declare no competing interest.
Received: February 8, 2024. **Accepted:** April 17, 2024.

feedforward nor commissural, GC wiring is inducible by Id2 (10, 14). Based on this, here, we hypothesized that the formation of the different MFS motifs is controlled by different molecular programs.

To test this hypothesis, we looked for GC transcriptomic differences between the KA model inducing all three MFS motifs (10, 11, 14) and the Id2 model inducing the feedback MFS motif (10). We identified bHLH TF Ascl4 and showed that the adeno-associated virus- (AAV-) mediated ectopic expression of Ascl4 (AAV–Ascl4) induces feedforward wiring in adult GCs. To test whether AAV–Ascl4 can induce wiring in other cell types, we extended our analysis to adult CA1 pyramidal cells (CA1 PYRs), which can also grow new axons in epilepsy models (1). We used comprehensive neuroanatomical, electrophysiological, and transcriptomic analyses to characterize Ascl4-induced wiring in GCs and CA1 PYRs, and behavioral phenotyping to study their consequences on learning and memory.

Results

Ascl4 in adult hippocampal GCs

To start with, we reanalyzed our patch-RNA-seq data (10) (GSE161619), consisting of a total of 248 single GC samples, for possible differences in the transcriptional regulation of KA and AAV–Id2-induced GC wiring (Fig. S1). We focused on bHLH TFs because of their potential role in adult wiring (1). Out of 107 bHLH TFs (16), 36 were expressed in at least 10 cells in at least one of the experimental groups (the group with the least cells containing 29 GCs), which we used as an arbitrary cutoff. Of the 36, 9 had significantly increased expression after KA but not after AAV–Id2. Based on STRING protein interaction analysis (17), it was found that 8 of the 9 bHLH TFs were directly associated with either Id2 or the transcriptional program inactivated by Id2 (10) (Fig. S1A–D). The only exception was Ascl4.

Next, we performed Ascl4 immunostaining after administering intra-hippocampal KA injection. In saline-injected controls, the Ascl4 immunosignal was relatively weak in most GCs; meanwhile, a few GCs were strongly labeled. In contrast, Ascl4 was strongly enriched in most GCs 1 day after KA, which persisted 14 days later (Figs. 1A, B and S1E). Ascl4 was nuclear, both after saline and after KA. This expression pattern was different from Id2, which was nuclear 1 day after KA but cytosolic later (10). While the Id2 localization was consistent with its presumed mechanism of action (i.e. binding and sequestering TFs to the cytosol to prevent their involvement in transcription or being sequestered to the cytosol by other factors) (18–22), its bHLH targets remained poorly characterized (5) and the different localizations of Ascl4 and Id2 at least suggested that Ascl4 is not a target of Id2. In addition, we did not find AAV–Id2-induced effects on the endogenous Ascl4 mRNA and protein levels (Fig. S1D and F), further supporting the hypothesis that Ascl4 and Id2 may function independently from each other.

Ascl4 induces axon growth in adult hippocampal GCs

To further investigate Ascl4, we cloned and ectopically expressed the Ascl4 gene in Cre-expressing ventral hippocampal GCs of adult Calb1-IRES-Cre-D mice using Cre-dependent AAVDJ/8 virus (referred to as AAV–Ascl4; Fig. 1C); to identify the injection site, AAV–EGFP was co-injected [for controls, only AAV–EGFP (enhanced green fluorescent protein) was injected in equal amount]. Three months later, we prepared acute brain slices for biocytin labeling and electrophysiological recording of the fluorescently labeled GCs (Fig. 1D).

First, we characterized morphological properties in the dentate gyrus and hilus, where GC axons and dendrites remained relatively well preserved in the brain slices. AAV–Ascl4 GCs had longer axons (AAV–EGFP: 1.54 ± 0.12 mm, $n = 26$ cells/9 mice, AAV–Ascl4: 1.93 ± 0.13 mm, $n = 30$ cells/8 mice; Welch's t test, $P = 0.028$) and more axonal branches (AAV–EGFP: 11 ± 0.83, AAV–Ascl4: 16 ± 1.40; Welch's t test, $P = 0.0048$) than controls (Fig. 1E; see Table S1 for sample/animal numbers and statistical data related to figures). While most axons extended into the hilus, indicating feedforward wiring, axons from 6 out of 30 (20%) AAV–Ascl4 GCs, but none of the controls, also entered the GC/inner molecular layers (GCL/IML; Fig. 1F) resembling feedback wiring. Although in a comparably smaller dataset, 4 of the 6 (67%) previously reconstructed AAV–Id2 GCs had axons in GCL/IML (10), highlighting a divergence between the wiring motifs induced by AAV–Ascl4 and AAV–Id2 (see also Fig. S2A and B). In addition, the total dendritic length of AAV–Ascl4 GCs decreased by ~12% (Fig. S2C; also see more below).

Second, to investigate possible effects in areas more distant than hilus, we analyzed GC axons, which could be at least partially recovered in CA3. On these, we did not observe AAV–Ascl4-induced effects on the density of mossy fiber boutons (MFBs; AAV–EGFP: 5 ± 0.63/mm, from $n = 9$ cells/5 mice; AAV–Ascl4: 4.8 ± 0.58/mm, from $n = 18$ cells/7 mice; Fig. 1G and H) or the surface area of MFBs (AAV–EGFP: 13 ± 0.84 μm^2, $n = 38$ MFBs, AAV–Ascl4: 11 ± 0.72 μm^2, $n = 57$ MFBs; Mann–Whitney U test, $P = 0.055$; Fig. 1I). In contrast, the MFB filopodia number increased (AAV–EGFP: 0.47 ± 0.16/MFB, AAV–Ascl4: 1.2 ± 0.19/MFB; Mann–Whitney U test, $P = 0.0045$; Fig. 1I). Consistent with the hypothesis that MFB filopodia number decreases with age (23), these numbers in 5- to 7-month-old mice were lower than in younger mice (2 weeks' old: ~7–13/MFB; 2 months' old: ~3/MFB) (23, 24). Nonetheless, based on a correlation between the structural complexity of MFBs and the GC synaptic output strength (24, 25), the increased filopodia number indicated potentially increased GC output after AAV–Ascl4 (see below). Further, in a separate experiment using retrograde labeling from the contralateral hippocampus, we tested whether AAV–Ascl4 induced commissural GC wiring as observed in the KA model (14). However, the number of retrogradely labeled GCs did not increase (Fig. S2D), suggesting that Ascl4 activation alone does not have the capacity to induce commissural axon growth.

Third, electrophysiological experiments showed that AAV–Ascl4 GCs had a more depolarized resting membrane potential, larger input resistance, and lower capacitance and fired more action potentials (APs) in response to steady-state current injections than controls (Fig. 1J–L). Previously, we also investigated these GC cellular properties in the AAV–Id2-induced wiring model, generating feedback GC wiring (10). Underscoring a divergence between the effects of Ascl4 and Id2, the GC resting membrane potential, capacitance, and AP firing were altered only by Ascl4 but not by Id2 (10), although the input resistance was similarly increased by both manipulations (Fig. 1K and Ref. (10)).

Together, these results indicated that differently from AAV–Id2, AAV–Ascl4 in adult GCs induced mainly feedforward wiring together with changes in neuronal excitability.

Ascl4 induces axon growth in adult hippocampal CA1 PYRs

Next, we tested whether the capacity of Ascl4 to induce axon growth was specific to GCs or whether AAV–Ascl4 also had the capacity to induce wiring in other adult cell types. We investigated this question by focusing on CA1 PYRs, which have also been shown to grow new axon collaterals in epilepsy models (26–30).

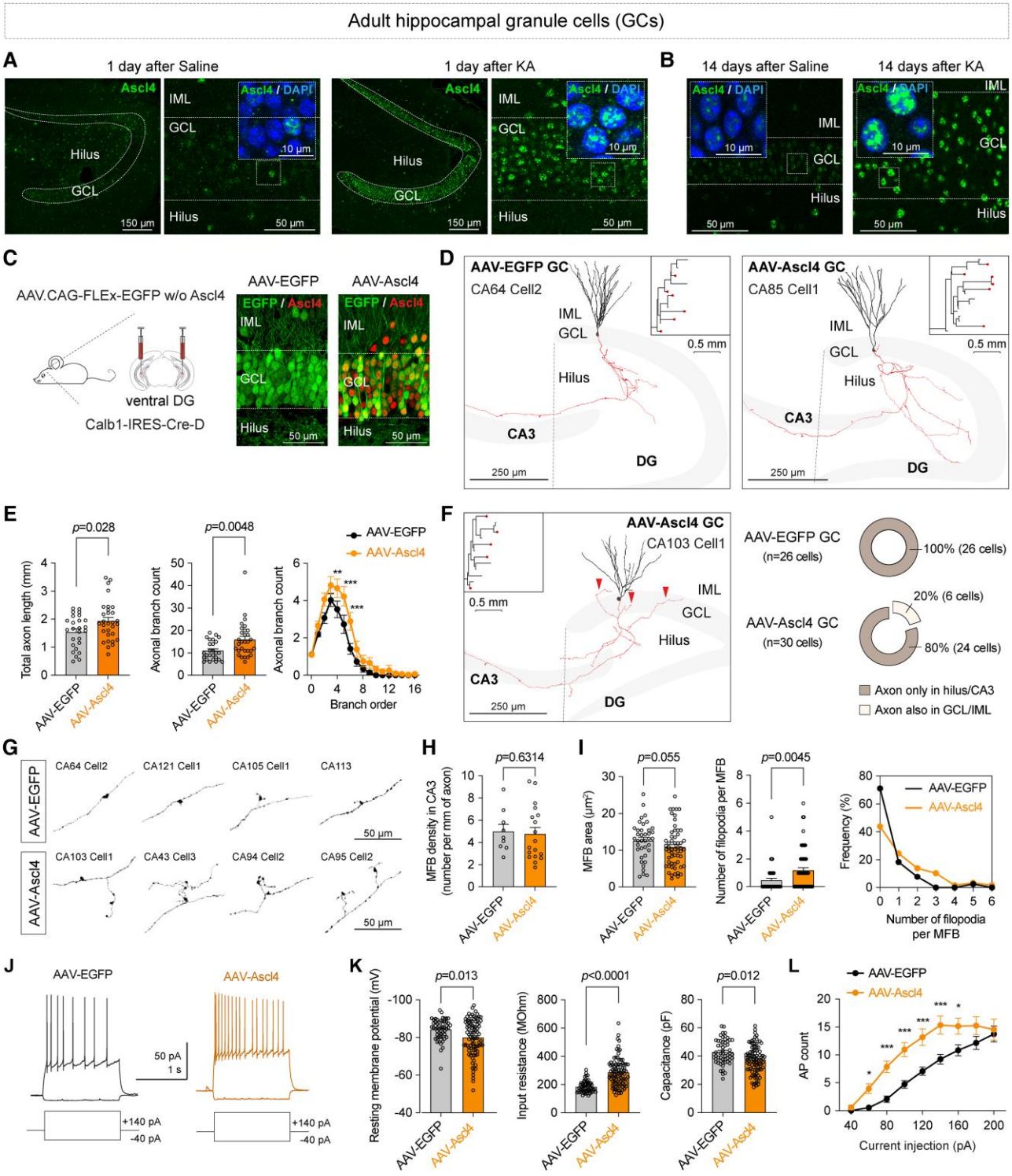

Fig. 1. Ascl4 induces axon growth in adult hippocampal GCs. A) Ascl4 immunostaining in 50-μm-thick brain sections 1 day after saline and KA injection. B) Ascl4 immunostaining 14 days after saline and KA. C) A schematic drawing of AAV targeting. The confocal images show Ascl4 immunostaining after AAV–EGFP and AAV–Ascl4. D) Example GCs after AAV–EGFP and AAV–Ascl4. Axons are shown in red, and somata and dendrites are shown in black. The dashed lines delineate the dentate/hilus area for axon morphological quantification. The insets show the axograms (red dots label branches exiting the slice surface). E) Quantification of the total axon length, branch count, and axonal branch count distribution of AAV–EGFP and AAV–Ascl4 GCs within the dentate/hilus 3 months after AAV injections. F) An example of an AAV–Ascl4 GC that had axons in GCL/IML (red arrowheads). The circle plots show the percentage of GCs with axons in GCL/IML. G) The images show MFBs and filopodia in CA3 (the main GC axons/mossy fibers extend in a left–right direction). H) Quantification of MFB density. I) Quantification of the MFB area, filopodia number, and filopodia number distribution (each circle represents a single MFB, and the data represent mean ± SEM across MFBs). J) Electrophysiological responses elicited by hyper- and depolarizing steady-state current injections in GCs. K) Resting membrane potential, input resistance, and capacitance of AAV–EGFP and AAV–Ascl4 GCs. L) AP counts evoked by 1.5-s long steady-state current injections in AAV–EGFP and AAV–Ascl4 GCs. In E, H, K, and L, each circle represents a single cell, and the data represent mean ± SEM across cells. *P ≤ 0.05, **P ≤ 0.01, ***P ≤ 0.001. See Table S1 for cell/sample/animal numbers and statistical details.

For this, we used adult Nex-Cre transgenic mice (31), in which, in the hippocampal CA1 area, Cre is exclusively expressed by PYRs. Three months after administering bilateral Cre-dependent AAV injections into ventral CA1, we prepared acute brain slices to analyze fluorescently labeled CA1 PYRs (Fig. 2A).

AAV–Ascl4 CA1 PYRs had longer axons (AAV–EGFP: 4.25 ± 0.40 mm, $n = 27$ cells/3 mice, AAV–Ascl4: 5.55 ± 0.40 mm, $n = 29$ cells/3 mice; Mann–Whitney U test, $P = 0.013$) and more axonal branches (AAV–EGFP: 22 ± 1.4, AAV–Ascl4: 27 ± 1.3; Welch's t test, $P = 0.012$) than controls (Fig. 2B and C). To examine whether AAV–Ascl4 uniformly induced axon growth in genetically diverse CA1 PYRs (32–34), we also stratified the cells based on their soma location in the proximal (closer to CA3), medial, or distal (closer to subiculum) CA1. Intriguingly, mostly medial and to a certain extent proximal, but not distal, CA1 PYRs were susceptible to AAV–Ascl4-induced axon growth (Fig. 2D). In addition, the apical, but not basal, dendritic length of medial AAV–Ascl4 CA1 PYRs decreased by ∼21%, whereas their apical, but not basal, dendritic branch count increased by ∼27% (Fig. S3; also see below).

With regard to electrophysiological properties, AAV–Ascl4 CA1 PYRs had a larger input resistance, but their resting membrane potential, capacitance, and AP firing did not display Ascl4-induced effects (Fig. 2E–G).

Ascl4-induced transcriptomic programs in GCs and CA1 PYRs

In order to identify the transcriptomic consequences of AAV–Ascl4, we performed patch-RNA-seq 1 month after AAV injections from GCs (53 AAV–EGFP and 52 AAV–Ascl4 GCs) and then from CA1 PYRs, mainly focusing on the medial population (48 AAV–EGFP and 51 AAV–Ascl4 CA1 PYRs; GSE246825). To augment our analyses, we again used our previous patch-RNA-seq data from GCs (51 AAV–EGFP and 59 AAV–Id2 GCs; Ref. (10); GSE161619).

First, we analyzed the GC transcriptome. Differential gene expression analysis revealed a significant (false discovery rate, FDR < 0.05) up-regulation of 771 and down-regulation of 739 genes in AAV–Ascl4 GCs compared with controls (Figs. 3A and S4A). STRING analysis of the top 50 up-regulated genes revealed a cluster associated with JAK-STAT (Stat1, Stat3, H2-D1, and Cd34) and interferon (Irf7, Isg15, Lgals3bp, Ifit1, Ifit3, and Rtp4) signaling (35–38) (Fig. S4B), and gene ontology (GO) analysis (39–41) of all significantly differentially expressed genes showed an enrichment of interferon signaling and catabolic processes (Fig. S4C).

Functionally, Ascl4 (a TF) directly, whereas Id2 (an inhibitor of TFs) indirectly, controls transcription. Phenotypically, AAV–Ascl4 induces mainly feedforward, whereas AAV–Id2 induces feedback wiring in GCs. Consistent with these functional and phenotypic differences, the Ascl4- and Id2-induced transcriptional programs were largely different (Fig. 3B). Differently regulated genes included synaptic cell surface receptors (Fig. S4D), which are generally important for target specification during wiring (13, 42–46). However, several genes were also co-regulated by Ascl4 and Id2 (Fig. 3B and C), 11 were up-regulated, and 3 were down-regulated, which we presumed would include a core program for adult GC wiring. Underscoring the notion of such a core program, the expression of 8 up-regulated genes (i.e. Stat1, Stat3, Ifit1, Ccl5, Cdkn1a, Irf1, Irf7, and Lgals3bp) was also similarly changed in the KA model (Fig. S5A and B; data from Ref. (10)), which induces feedback, feedforward, and commissural motifs.

Second, we analyzed the CA1 PYR transcriptome. We found a significant up-regulation of 80 genes and down-regulation of 150 genes in AAV–Ascl4 CA1 PYRs compared with controls (Figs. 3D and S6A)—comparably fewer than in GCs, potentially reflecting that the overall transcriptomic effect of Ascl4 depends on the gene regulatory landscape of the cell. STRING analysis identified a cluster associated with interferon signaling (Irf7, Ifi27l2a, Lgals3bp, Xaf1, Bst2, H2-K1, Ccl5, and Cd74; Fig. S6B), and GO analysis showed an enrichment of biosynthetic processes (Fig. S6C). Furthermore, these analyses revealed that AAV–Ascl4 did not alter endogenous Id2 expression in GCs or CA1 PYRs (Fig. 3A–D).

Finally, since Ascl4 induced wiring both in GCs and in CA1 PYRs, we looked for co-regulated genes: 12 genes were commonly up-regulated and 15 were down-regulated after AAV–Ascl4 in both cell types (Fig. 3E and F). The up-regulated genes included Irf7, Lgals3bp, and Ccl5, which were also up-regulated in AAV–Id2 GCs (Fig. 3B and C). Other genes (e.g. Stat1) did not reach FDR significance in AAV–Ascl4 CA1 PYRs as they did in GCs, but were still significantly up-regulated by non-adjusted $P < 0.05$ (Fig. 3E). Therefore, we analyzed a broader set of co-regulated genes ($P < 0.05$ and fold-change >2) in the AAV–Ascl4 (in GCs and CA1 PYRs) and AAV–Id2 (in GCs) wiring models: 9 genes were commonly up-regulated (Ccl5, H2-D1, Irf1, Irf7, Isg15, Lgals3bp, Pcyox1, Selenon, and Stat1) and 5 were down-regulated (C2cd4b, Esf1, Neil, Myo5b, and Tle1; Fig. 3G–J). Intriguingly, 5 of the 14 co-regulated genes (Esf1, Irf1, Irf7, Stat1, and Tle1) were TFs or transcriptional regulators, highlighting a striking convergence of Ascl4- and Id2-activated programs at the basic level of transcription.

Learning and memory after AAV–Ascl4

Thus far, our results indicate that AAV–Ascl4 induces wiring and biophysical changes in adult neurons. An important question is whether these changes impact circuit operations. To investigate whether the increased wiring and excitability of GCs and CA1 PYRs correlates with learning and memory impairments as observed in the experimental models of temporal lobe epilepsy (47–49), we performed hippocampus-dependent learning and memory tests. For this, we bilaterally injected AAVs both in the dorsal and in the ventral hippocampus of either adult male Calb1–Cre mice to induce wiring in GCs (13 AAV–EGFP and 15 AAV–Ascl4 mice) or Nex-Cre mice to induce wiring in CA1 PYRs (11 AAV–EGFP and 11 AAV–Ascl4 mice). We refer to the four groups as GC^{EGFP}, GC^{Ascl4}, PYR^{EGFP}, and PYR^{Ascl4} mice, for short. GC and PYR mice were tested separately and statistical comparisons were made only between the corresponding groups (Fig. 4A). Three months after AAV injections, we performed the following order of behavioral tests: home cage activity monitoring, open field, novel object location, novel object recognition, elevated O-maze, light–dark box, eight-arm radial maze, Morris water maze, and fear conditioning.

Home cage monitoring (12:12 h light–dark cycle) showed that GC^{Ascl4} and PYR^{Ascl4} mice increased their activity at the onset of the dark phase compared with their controls (Figs. 4B and S7A). In addition, PYR^{Ascl4} mice were generally more active during the dark phase (Fig. 4B) and their increased activity was also evident in the open field test (Fig. 4C). The novel object location and recognition tests did not reveal phenotypic changes in the GC^{Ascl4} and PYR^{Ascl4} mice (Fig. S7B–E). In the elevated O-maze, mice generally showed initial exploration, followed by robust habituation (i.e. their travel distance progressively decreased during the observation), and the only exception was the PYR^{Ascl4} group, which did not display significant habituation (Fig. 4D). Further, canonical anxiety measures such as place preference in the open field (Fig. S7C), elevated O-maze (Fig. S7F), and light–dark box tests

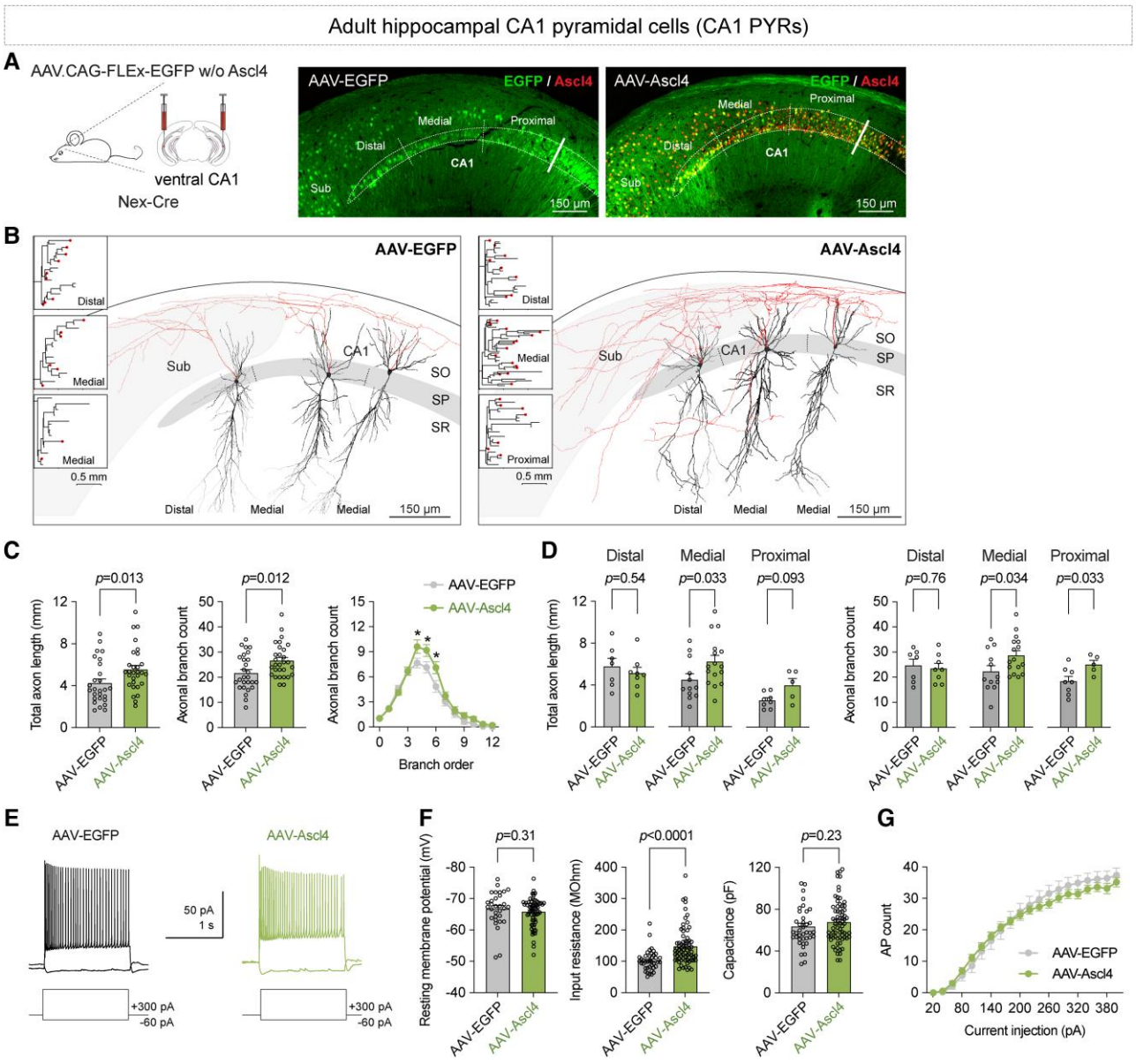

Fig. 2. Ascl4 induces axon growth in adult hippocampal CA1 PYRs. A) A schematic drawing of AAV targeting. The confocal images show Ascl4 immunostaining after AAV–EGFP and AAV–Ascl4, and stratification of proximal, medial, and distal CA1 areas. B) Example proximal, medial, and distal AAV–EGFP and AAV–Ascl4 CA1 PYRs. Axons are shown in red, and somata and dendrites are shown in black. The insets show the axograms (red dots label branches exiting the slice surface). SO, str. oriens; SP, str. pyramidale; SR, str. radiatum; Sub, subiculum. C) Quantification of the total axon length, branch count, and axonal branch count distribution of AAV–EGFP and AAV–Ascl4 CA1 PYRs 3 months after AAV injections. D) The total axon length and axonal branch count of distal, medial, and distal CA1 PYRs. E) Electrophysiological responses elicited by hyper- and depolarizing steady-state current injections in CA1 PYRs. F) Resting membrane potential, input resistance, and capacitance of AAV–EGFP and AAV–Ascl4 CA1 PYRs. G) AP counts evoked by 1.5-s long steady-state current injections in AAV–EGFP and AAV–Ascl4 CA1 PYRs. In C, D and F, G, each circle represents a single cell, and the data represent mean ± SEM across cells. $^*P \leq 0.05$. See Table S1 for cell/animal numbers and statistical details.

(Fig. S7G) did not provide support for anxiety-related phenotypic changes neither in the GC^{Ascl4} nor in the PYR^{Ascl4} mice.

In the eight-arm radial maze test, GC^{Ascl4} and PYR^{Ascl4} mice made the same number of correct choices as their controls. However, PYR^{Ascl4} but not GC^{Ascl4} mice increased their memory errors (entering an arm and looking for a food pellet, or bait, which was already consumed) at the expense of procedural errors (entering and leaving an arm without looking for an already consumed bait) (Fig. 4E). This effect was apparent after the mice already collected 5–6 (of 8 total) baits on any day of the test (Figs. 4E and S7H), suggesting that an increased memory load prevented further improvements with training in PYR^{Ascl4} mice. The results from the Morris water maze test corroborated these findings. Although GC^{Ascl4} and PYR^{Ascl4} mice learned equally well during acquisition as their controls, the PYR^{Ascl4} mice but not the GC^{Ascl4} mice displayed longer escape latencies and swim paths during the second day of reversal learning (Figs. 4F and S7I). Finally, fear conditioning did not reveal generalized freezing by the GC^{Ascl4} and PYR^{Ascl4} mice, nor deficits in their context and cue retention (Fig. 4G).

Taken together, comprehensive behavioral phenotyping did not reveal pathological impairment in the primary task performance of GC^{Ascl4} and PYR^{Ascl4} mice, but highlighted a potential spatial reference memory impairment in the PYR^{Ascl4} mice with increasing memory load.

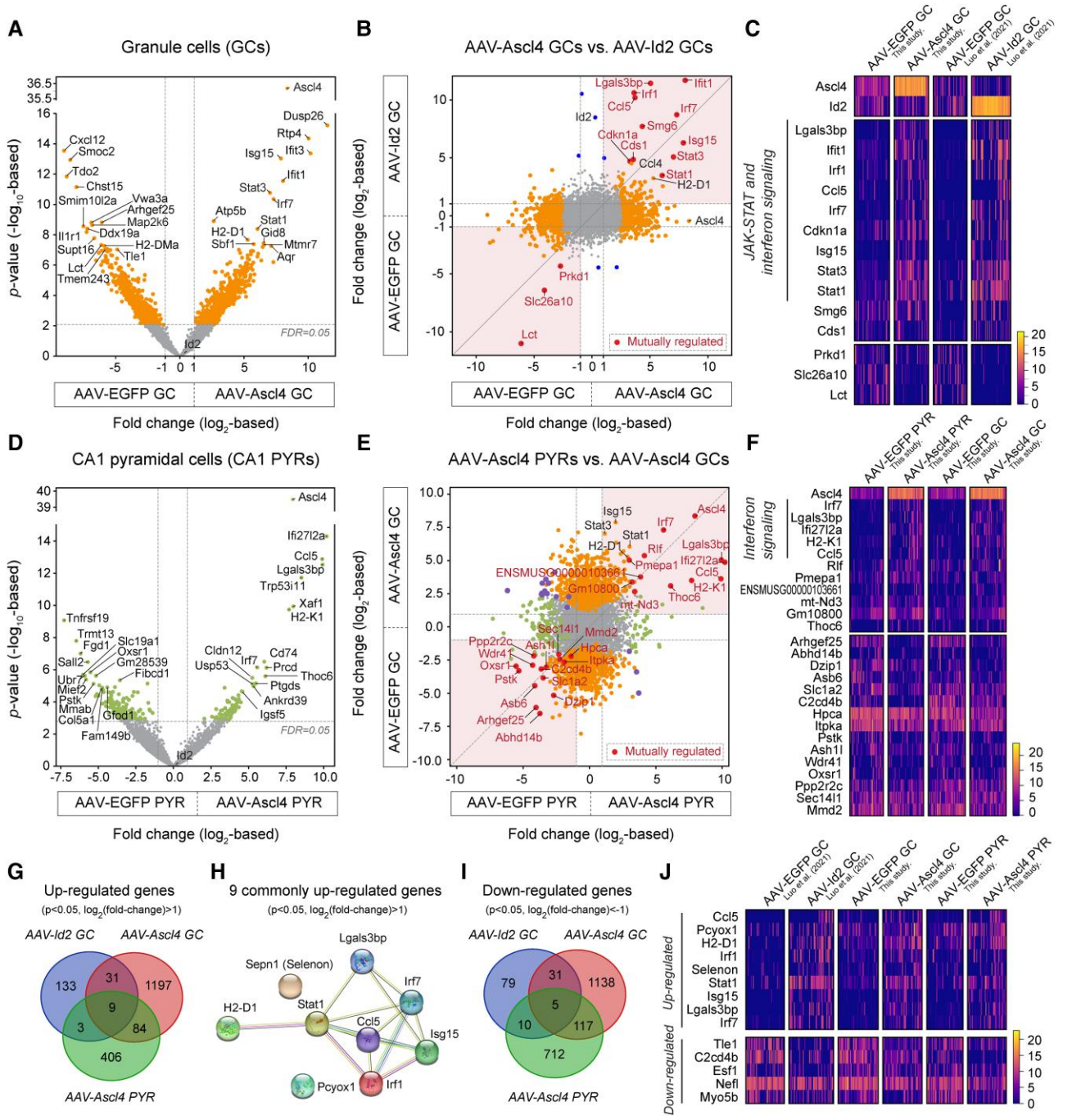

Fig. 3. Ascl4-induced transcriptomic programs in adult GCs and CA1 PYRs. A) The volcano plot shows a differential gene expression between AAV–EGFP and AAV–Ascl4 GCs. Vertical dashed lines: $|\log_2(\text{fold-change})| = 1$, horizontal dashed line: FDR = 0.05. B) Correlated gene expression changes in GCs after AAV–Ascl4 (horizontal axis) and AAV–Id2 (vertical axis). Genes colored with: gray = not significantly changed by either manipulation; blue = regulated by AAV–Id2; orange = regulated by AAV–Ascl4; red = mutually co-regulated by AAV–Ascl4 and AAV–Id2. C) The heat map shows the expression of Ascl4 and Id2, and mutually regulated genes by AAV–Ascl4 and AAV–Id2 (red-labeled genes in B). The scale bar is $\log_2(\text{TPM} + 1)$. D) Differential gene expression between AAV–EGFP and AAV–Ascl4 CA1 PYRs. E) Correlated gene expression changes in CA1 PYRs (horizontal axis) and GCs (vertical axis) after AAV–Ascl4. Gray = not significantly changed in either cell type; green = regulated in CA1 PYRs; orange = regulated in GCs; red = mutually co-regulated in GCs and CA1 PYRs; purple = oppositely regulated in GCs and CA1 PYRs. F) The heat map shows mutually regulated genes in AAV–Ascl4 GCs and AAV–Ascl4 CA1 PYRs (red-labeled genes in E). G) The Venn diagram shows the number and intersection of up-regulated genes in AAV–Ascl4 GCs, AAV–Id2 GCs, and AAV–Ascl4 CA1 PYRs. H) The STRING protein network analysis shows a functional association among the nine mutually up-regulated genes in G. I) Down-regulated genes in AAV–Ascl4 GCs, AAV–Id2 GCs, and AAV–Ascl4 CA1 PYRs. J) The heat map shows the expression of mutually up-regulated ($n = 9$) and down-regulated ($n = 5$) genes in AAV–Ascl4 GCs, AAV–Id2 GCs, and AAV–Ascl4 CA1 PYRs.

Circuit properties in the GC^{Ascl4} and PYR^{Ascl4} mice

Five months after AAV injections and after the behavioral tests, we prepared acute brain slices from the ventral hippocampus for morphological and electrophysiological analyses. Although the experimental conditions between the data collected 3 (Figs. 1 and 2) and 5 months (Fig. 5) after the AAV injections differed in key aspects (3 months: ventral AAV injections without behavioral tests, 5 months: ventral/dorsal

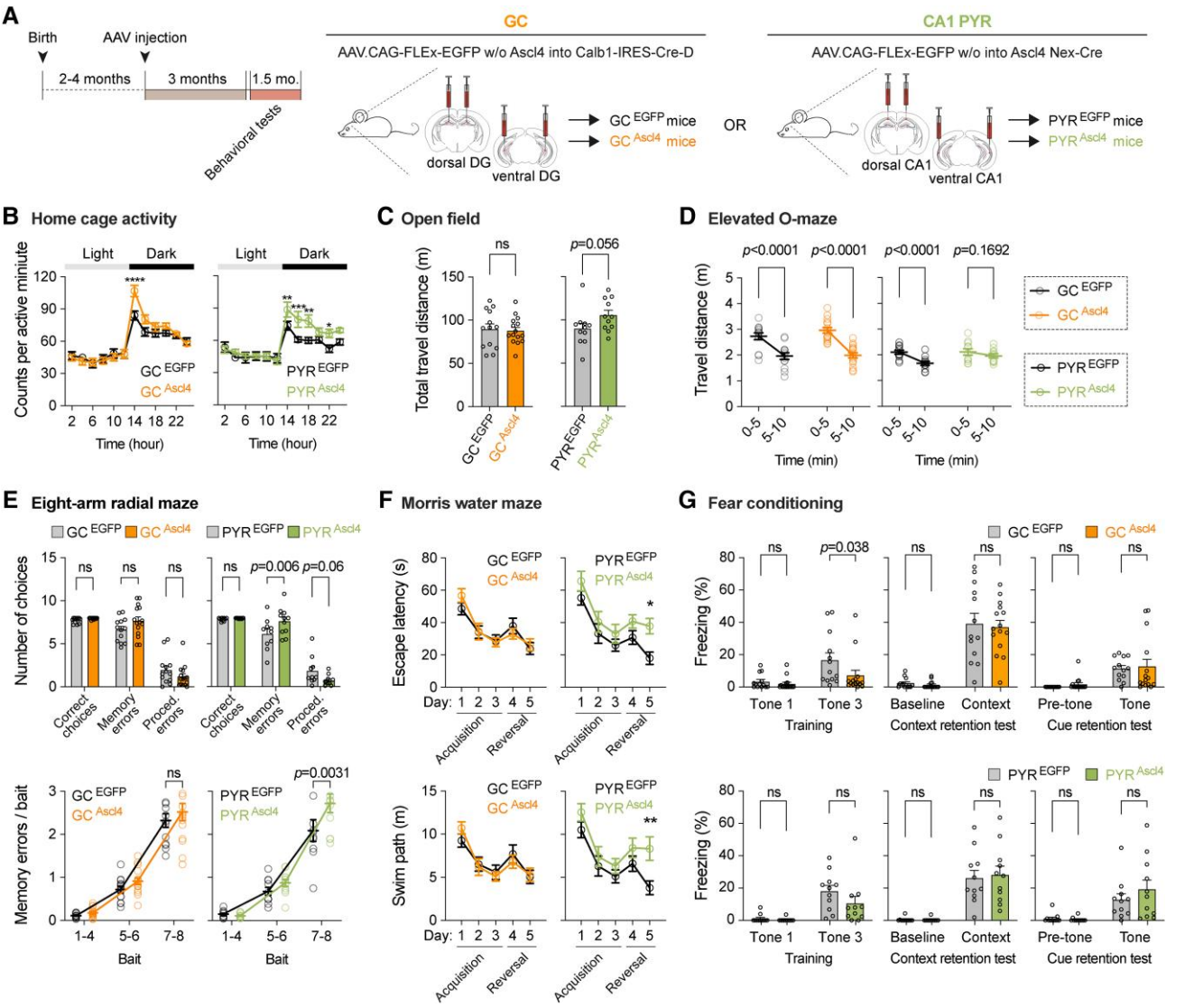

Fig. 4. Learning and memory after AAV–Ascl4. A) An experimental schedule for GC^{EGFP} and GC^{Ascl4}, and PYR^{EGFP} and PYR^{Ascl4} mice. B) Home cage activity. The plots show activity counts in 2-h time segments during light and dark phases. C) Open field. The plot shows the total distance traveled. D) Elevated O-maze. The plots show the travel distance in the first (0–5) and second (5–10) 5 min of the test. E) Eight-arm radial maze. The upper plots show the distribution of correct choices, memory errors, and procedural errors. The lower plots show memory errors per consumed baits. F) Morris water maze. The upper plots show the escape latency, and the lower plots show the length of the swim path during acquisition and reversal days. G) Fear conditioning. The plots show the quantification of freezing time, as a percentage of the total observation time is shown during the fear conditioning training, context retention test, and cue retention test. In B and F, the data represent mean ± SEM across animals. In C–E and G, each circle represents a single animal, and the data represent mean ± SEM across animals. $^{*}P \leq 0.05$, $^{**}P \leq 0.01$, $^{***}P \leq 0.001$, $^{****}P \leq 0.0001$. See Table S1 for animal numbers and statistical details.

AAV injections followed by behavioral tests), we cross-referenced these data to identify lasting consequences of AAV–Ascl4.

First, we analyzed the GC^{EGFP} and GC^{Ascl4} mice after 5 months and confirmed the wiring phenotype found after 3 months: GCs in the GC^{Ascl4} mice had longer axons and more axonal branches than in GC^{EGFP} mice (Figs. 5A and S8A). GCs in the GC^{Ascl4} mice also had larger input resistance and lower capacitance (Fig. S8C); however, unlike after 3 months, we did not find Ascl4-induced changes in their dendritic length and AP firing (Fig. S8B and C), suggesting that these effects were transient. To investigate GC synaptic inputs, we recorded spontaneous EPSCs (sEPSCs; in the presence of 10 µM Gabazine) from GCs, which did not display Ascl4-induced changes (Fig. S8D). To investigate GC outputs, we first recorded sEPSCs from hilar neurons representing a combination of interneurons and mossy cells (the identity of these cell types could not be unequivocally distinguished in these recordings). Intriguingly, both the frequency and amplitude of sEPSC were lower in GC^{Ascl4} hilar neurons (Fig. 5B), indicating that GC wiring in the hilus does not necessarily lead to increased, but decreased, synaptic efficacy. To further study GC outputs, we then analyzed the GC to CA3 PYR transmission using the same approach as in our previous study (10): we electrically stimulated the perforant path to activate GCs and recorded GC-evoked EPSCs (eEPSCs; in the presence of 10 µM Gabazine) from CA3 PYRs. We found a ~2-fold increase in eEPSC amplitude (GC^{EGFP}: 1,042 ± 159 pA, $n = 18$ cells/3 mice, GC^{Ascl4}: 1,996 ± 181 pA, $n = 19$ cells/3 mice; Mann–Whitney U test, $P = 0.0007$) and decay time (GC^{EGFP}: 70 ± 9.0 ms, GC^{Ascl4}: 128 ± 18 ms, Mann–Whitney U test, $P = 0.0029$) in the GC^{Ascl4} mice (Fig. 5C). Of note, we did not find AAV–Id2-induced effects on the GC to CA3 PYR transmission in our previous study (10).

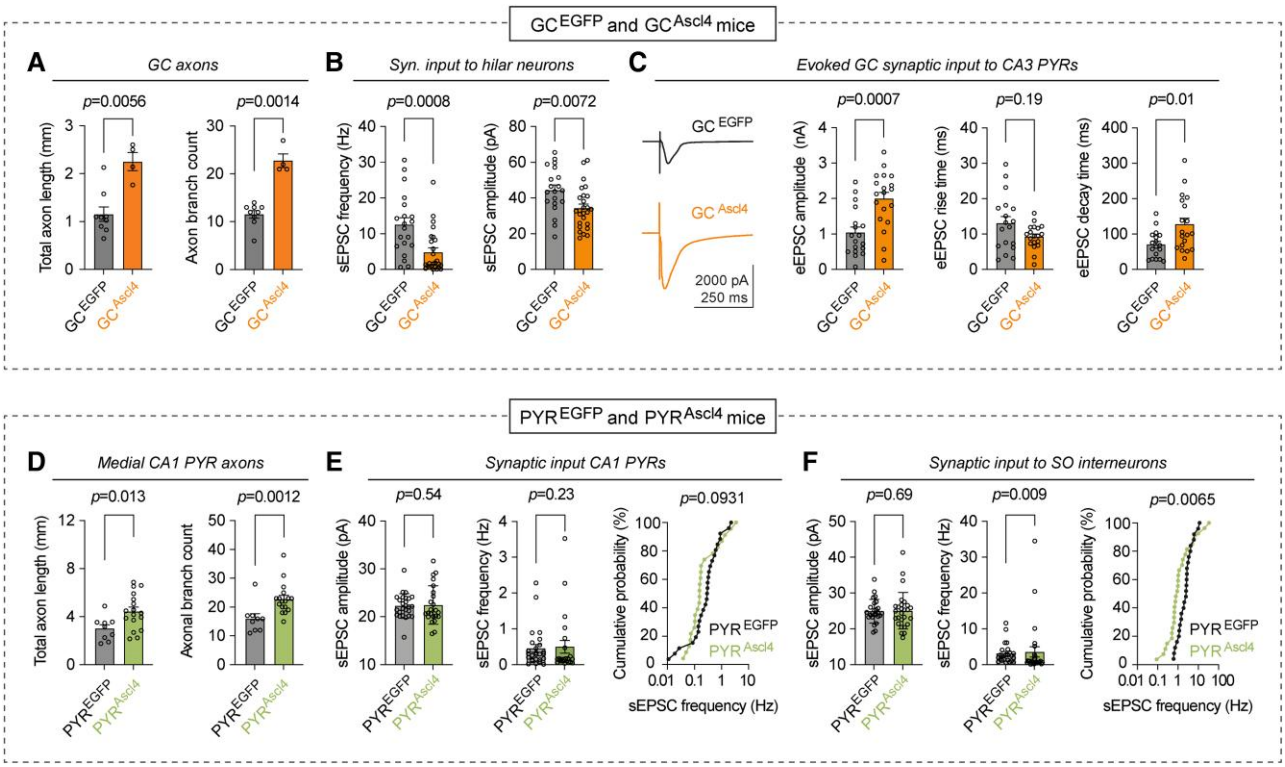

Fig. 5. Circuit analyses after AAV–Ascl4. A) The plots show GC axon length and branch count in the GC^{EGFP} and GC^{Ascl4} mice 5 months after AAV injections. B) sEPSC frequency and amplitude recorded from hilar neurons in the GC^{EGFP} and GC^{Ascl4} mice. C) The example traces show eEPSCs recorded from CA3 PYRs in the GC^{EGFP} and GC^{Ascl4} mice. The plots show eEPSC amplitude and the rise and decay times. D) The plots show medial CA1 PYR axon length and branch count in the PYR^{EGFP} and PYR^{Ascl4} mice 5 months after AAV injections. E) sEPSC amplitude, frequency, and cumulative probability of sEPSC frequencies recorded from CA1 PYRs in the PYR^{EGFP} and PYR^{Ascl4} mice. F) sEPSC amplitude, frequency, and cumulative probability of sEPSC frequencies recorded from SO interneurons in the PYR^{EGFP} and PYR^{Ascl4} mice. In A and D, each circle represents a single cell, and the data represent mean ± SEM. In B, C and E, F, each circle represents the measured parameter (frequency) or the mean measured parameter (amplitude) from a single cell, and the data represent mean ± SEM. See Table S1 for cell/animal numbers and statistical details.

Second, we analyzed the PYR^{EGFP} and PYR^{Ascl4} mice after 5 months and confirmed the wiring phenotype seen after 3 months: medial CA1 PYRs in the PYR^{Ascl4} mice had longer axons and more axonal branches than their controls (Figs. 5D and S9A, B). However, their dendritic length and branch count were not any different from controls (Fig. S8C). Also, similar to 3 months, CA1 PYRs in the PYR^{Ascl4} mice had larger input resistance (Fig. S8D). To investigate synaptic properties, we recorded sEPSCs from CA1 PYRs and interneurons in the stratum oriens (SO). Although the connectivity between CA1 PYRs is sparse in the naive brain (50, 51), we presumed that new axons could feasibly form connections with other CA1 PYRs; meanwhile, SO interneurons are a major target of CA1 PYRs in the naive brain (51). We did not observe a change in the sEPSC amplitudes recorded from CA1 PYRs; however, the cumulative probability distribution of the frequencies showed a decreasing shift in the PYR^{Ascl4} mice compared with PYR^{EGFP} (Fig. 5E). This effect was more pronounced in SO neurons, where the cumulative probability distribution of sEPSC frequencies was significantly different between PYR^{EGFP} and PYR^{Ascl4}, most cells receiving less excitatory inputs (Figs. 5F and S9E).

Together, these analyses revealed lasting AAV–Ascl4-induced morphological and biophysical changes in GCs and CA1 PYRs, as well as altered synaptic properties in the circuit.

Discussion

To understand wiring regulation in adults, we investigated wiring permissive molecular programs in adult hippocampal neurons. Our study was motivated by the hypothesis that feedback, feedforward, and commissural MFS are regulated by different transcriptional programs. Previously, we found that Id2 can induce feedback wiring in GCs (10). The goal of this study was to identify the regulator(s) of the feedforward and/or commissural wiring. Our study addressed this goal in GCs and extended the applicability of the findings to CA1 PYRs. Our results have major implications for understanding wiring and circuit assembly in the adult brain and the pathomechanisms of epilepsy.

Ascl4 induces axon growth in adult neurons

We first identified Ascl4 as a key regulator that can cell-autonomously induce feedforward wiring in GCs (Fig. 6). To date, Ascl4 has not been implicated in neuronal function or wiring. In addition to feedforward wiring, AAV–Ascl4 induced biophysical changes that were different from those produced by Id2 (10). These observations suggest that Ascl4 and Id2 differently control transcription. To broaden our scope, we asked whether Ascl4 can induce wiring in other cell types, and whether the corresponding transcriptional changes would be similar to those in GCs. The CA1 PYR experiments positively answered both questions (Fig. 6).

In response to AAV–Ascl4, we detected the generation of ~0.5–1 mm new axons per hippocampal neuron. Considering that AAVs may infect up to 20,000–30,000 cells, we estimate the addition of ~10–30 m of new axons to each hippocampus. Cell labeling in hippocampal slices, however, does not account for new interlamellar

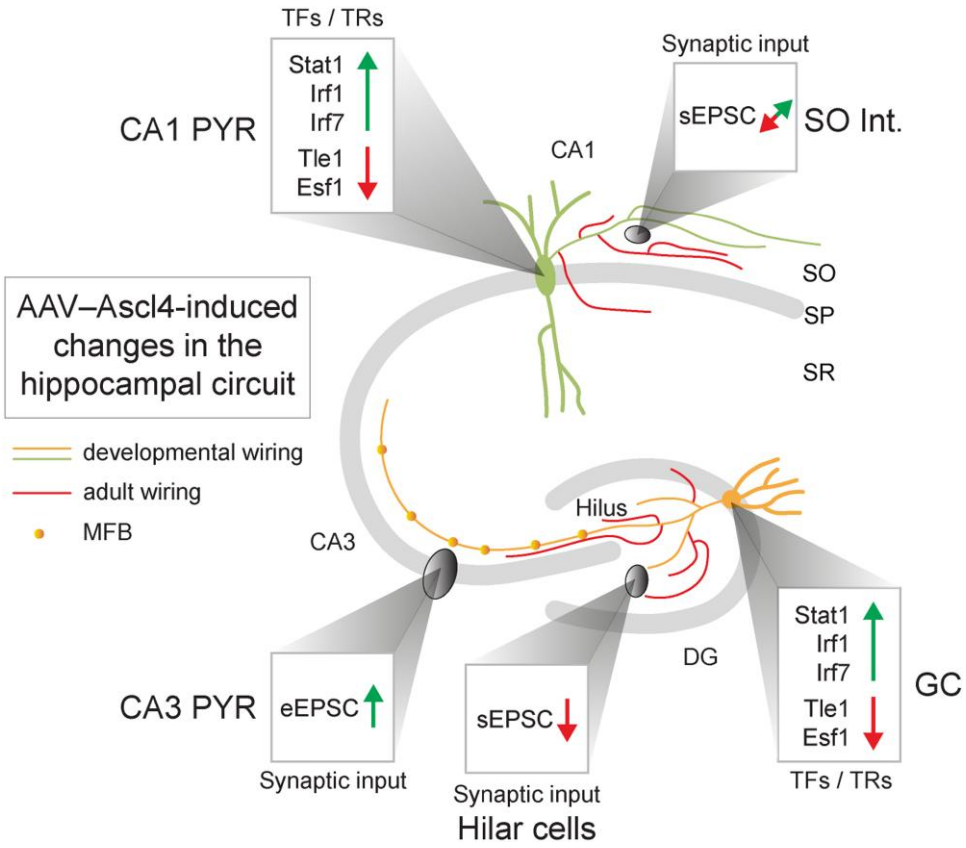

Fig. 6. A graphic summary of the effects of AAV–Ascl4 in different adult hippocampal neurons. The diagram depicts AAV–Ascl4-induced transcriptomic (commonly regulated TFs and transcriptomic regulators) and axon morphological effects in adult GCs and CA1 PYRs, as well as synaptic changes in their output neuronal populations.

hippocampal or extra hippocampal wiring. The latter may be especially relevant for CA1 PYRs, which innervate multiple distant areas in the naive brain (32, 52, 53).

Transcriptional programs for adult wiring

To investigate the underlying molecular programs, we performed two principal analyses. First, to identify co-regulated genes during feedforward and feedback GC wiring, we compared gene expression changes induced by AAV–Ascl4 and AAV–Id2 in GCs. Second, to examine whether the Ascl4 program was conserved, we compared gene expression changes induced by AAV–Ascl4 in GCs and CA1 PYRs. The first analysis revealed that synaptic cell surface/adhesion molecules that are important for target specification during wiring (13, 42–46) were differently regulated (Fig. S4D), and that the AAV–Ascl4-induced changes were more pronounced than those by AAV–Id2. Associated with axon growth, synapse formation, and/or synapse regulation, Pcdh17 (54), Lrrtm3 (55, 56), Adgrl3 (57, 58), Ctnnb1 (59, 60), Epha4 (61), Clstn2 (62), Ptpro (63), Nrxn3 (64, 65), Sema4f (66), and Nptn (67) were up-regulated by Ascl4. In contrast, associated with growth cone collapse, synapse stabilization, and/or synapse elimination, Il1r1 (68), the complex forming Ncam and Epha3 (69, 70), Ephb1 (71), Clql2 and C1ql3 (64), Slitrk2 (72), Cdh2 and Cdh8 (73–75), Sema5a (76), Mdga2 (77, 78), and Sdc3 (79) were down-regulated by Ascl4. With relevance to GCs and CA1 PYRs, several of these molecules have been characterized in the mossy fiber system (Lrrtm3 (56), Ctnnb1 (59), Epha4 (61), Nrxn3 (64, 65), Ephb1 (72), C1ql2 and C1ql3 (64), Cdh2 and Cdh8 (73), Sema5a (76), and Sdc3 (79)) or hippocampal principal cells (Adgrl3 (57, 58), Ctnnb1 (60), Clstn2 (62), Prpro (63), Sema4f (66), Slitrk2 (72), and Mdga2 (77, 78)). Meanwhile, these molecular changes suggest that AAV–Ascl4 reactivated a transcriptomic GC program for circuit plasticity, the precise involvement of these molecules in feedforward wiring, or more broadly, in the distinction between the Ascl4- and Id2-dependent wiring motifs, remains to be determined.

In contrast to the differentially regulated genes, a comparably smaller set of genes was co-regulated by Ascl4 and Id2. These genes were mostly associated with JAK-STAT and interferon signaling, which have been associated with axon growth and regeneration (10, 80–83). It is, therefore, plausible that differently regulated genes control the formation of distinct circuit motifs, whereas co-regulated genes control the shared features of wiring, such as axon growth. The second analysis revealed that several of the Ascl4/Id2 co-regulated GC genes were similarly regulated by Ascl4 in CA1 PYRs (Fig. 6). Stat1 was commonly up-regulated, suggesting that STAT activation may be a key step in adult wiring. The interferon regulatory factor (IRF) Irf1 and chemokine Ccl5 were also up-regulated. Irf1 expression is feasibly driven by Stat1, but after it is up-regulated, Irf1 may also associate with Stat1 to expand the Stat1 genomic-binding profile to IRF-binding sites (38, 84); meanwhile, Ccl5 has been shown to mediate retinal development and promote optic nerve regeneration (85, 86). In contrast, Tle1, a co-repressor of the axon patterning Wnt signaling (87, 88), and Nefl, which determines mature axon structure and caliber (89), were down-regulated, potentially increasing a capacity for axonal plasticity.

Taken together, our results indicate that adult wiring is transcriptionally controlled. Although insights into the post-transcriptional regulation of Ascl4- and Id2-controlled genes remain scarce, our transcriptomic results corroborate a plausible model by which Ascl4 or Id2 induce STAT expression, the downstream targets/effectors of which may inhibit Rho/Rock signaling to allow axon elongation (1).

Finally, insights into multiple questions remain limited by the scope of this current study. First, given that we identified Ascl4 and Id2 in the KA model and used an AAV approach to study them, both leading to exaggerated expression levels, the physiological role of Ascl4 and Id2 in the regulation of wiring remains elusive. Second, the question of whether Ascl4 and Id2 are required only for wiring induction or also for the maintenance of new circuits remains open. Addressing these conceptually important problems will require updated study designs that employ conditional inducible and/or knockout transgenic lines and proteomic/functional assays.

Hippocampal function after AAV–Ascl4 induction

Although axonal sprouting by GCs (10, 11, 14) and CA1 PYRs (26–30) has been characterized in experimental models of temporal lobe epilepsy, their specific contribution to the disorder remains elusive. Our ability to genetically induce wiring in these cell types without other epilepsy-associated pathologies, such as cell dispersion or death, allowed us to investigate this problem.

Overall, the GC^{Ascl4} and PYR^{Ascl4} mice did not display deficits in primary task performance and learned equally well as their controls. Epilepsy-associated learning and memory impairments (such as in object location memory, Barnes and Morris water maze tests) (47–49) were not apparent. Of note, recurrent GC wiring induced by AAV–Id2 also did not elicit primary task performance deficits (10). Nonetheless, PYR^{Ascl4}, but not GC^{Ascl4}, mice displayed secondary task performance deficits in the eight-arm radial and Morris water maze, which could be potentially interpreted as increased memory load in these animals.

Subsequent circuit analyses confirmed lasting neuronal changes 5 months after AAV injections: the axon length and branch number of GCs and medial CA1 PYRs increased compared with controls. In addition, multiple synaptic changes characterized the hippocampal circuit (Fig. 6). As a potentially shared consequence of AAV–Ascl4 in different cell types, the synaptic drive on certain neuronal output populations decreased. However, the synaptic changes were context dependent. In GC^{Ascl4} hilar neurons, the lower frequency of sEPSCs corresponded with decreased amplitudes. In PYR^{Ascl4} SO and to a certain extent CA1 PYR neurons, a decreasing shift in the frequency distribution of sEPSCs indicated a decrease in synaptic excitation. In addition, our recordings revealed evidence for increased synaptic drive after AAV–Ascl4: the GC input strength to GC^{Ascl4} CA3 PYRs has increased by ∼2-fold compared with controls. This powerful synaptic phenotype correlated with a ∼2-fold increase in MFB filopodia number, which may provide support for the hypothesis that they are a key structural determinant of GC to CA3 PYR synapses (24, 25). However, alternative scenarios should also be considered, such as a potential increase in the number of active zones or readily releasable vesicles, which we did not investigate but could feasibly contribute to increase GC to CA3 PYR transmission. Furthermore, the increased MFB filopodia number may lead to increased activation of CA3 interneurons, the classically characterized targets of filopodia (90), and, as a consequence, increase feedforward inhibition of CA3 PYRs.

Overall, our results indicate that the synaptic changes elicited by Ascl4 are cell-type specific. It is feasible that different phenotypes reflect differential transcriptional regulation of synaptic molecules in the manipulated neurons. However, our data cannot rule out the possibility of homeostatic adaptations either, which may appear in response to the altered connectivity and/or excitability of the manipulated neurons. Both GCs and CA1 PYRs innervate multiple different cell types, including different types of interneurons, and Ascl4-induced synaptic changes to any of these could change information routing in the network. Elucidating the specific changes in each synapse type would clearly help to understand the mechanisms of adult wiring. Irrespective of this goal, the lack of impairments in the primary task performance of the animals suggests that the Ascl4-induced axonal, biophysical, and synaptic changes in GCs or CA1 PYRs do not elicit uncompromising pathophenotypes, increasing hopes that harnessing adult wiring could have beneficial therapeutic value in the future.

Summary

Our results demonstrate reprogrammed wiring in healthy adult neurons by a single TF. A more detailed understanding of how Ascl4 and the molecules it controls contribute to this process could potentially help one to understand how brain connectivity is regulated across the lifespan and facilitate the development of circuit therapies to alleviate the detrimental consequences of brain disorders characterized by the loss of neuronal connections.

Methods

Experimental protocols and husbandry practices were approved by the Veterinary Office of Zürich Kanton. For a comprehensive description of (i) animals, (ii) plasmids and viruses, (iii) stereotaxic injections, (iv) single-cell RNA-seq and bioinformatics, (v) histology and neuroanatomy, (vi) electrophysiology, and (vii) behavior, see the SI Appendix.

Acknowledgments

The authors thank Drs Jean-Charles Paterna and Melanie Rauch of the Neuroscience Center Zurich (ZNZ) for discussions and virus production, and the Functional Genomics Center Zurich (FGCZ) for RNA sequencing support. Imaging was performed with equipment maintained by the Center for Microscopy and Image Analysis, University of Zurich.

Supplementary Material

Supplementary material is available at *PNAS Nexus* online.

Funding

This study was supported by the Swiss National Science Foundation (310030_188506 and 310030_219390, C.F.), Dr Eric Slack-Gyr-Stiftung (C.F.), and Novartis Stiftung für medizinisch-biologische Forschung (20A022, C.F.).

Author Contributions

W.L. and C.F. designed the research; W.L., M.E., N.C.-O., A.T., G.M., B.T., D.L., C.S., I.A., T.L., and D.W. performed the research and analyzed data; C.F. wrote the paper.

Data Availability

The RNA-seq data have been deposited in the National Center for Biotechnology Information Gene Expression Omnibus (GSE246825).

References

1 Seng C, Luo W, Földy C. 2022. Circuit formation in the adult brain. *Eur J Neurosci*. 56(3):4187–4213.
2 Langlands K, Yin X, Anand G, Prochownik EV. 1997. Differential interactions of Id proteins with basic-helix-loop-helix transcription factors. *J Biol Chem*. 272(32):19785–19793.
3 Ruzinova MB, Benezra R. 2003. Id proteins in development, cell cycle and cancer. *Trends Cell Biol*. 13(8):410–418.
4 Murre C. 2019. Helix-loop-helix proteins and the advent of cellular diversity: 30 years of discovery. *Genes Dev*. 33(1–2):6–25.
5 Torres-Machorro AL. 2021. Homodimeric and heterodimeric interactions among vertebrate basic helix-loop-helix transcription factors. *Int J Mol Sci*. 22(23):12855.
6 Yu P, *et al.* 2011. Inhibitor of DNA binding 2 promotes sensory axonal growth after SCI. *Exp Neurol*. 231(1):38–44.
7 Ko HR, *et al.* 2016. Akt1-inhibitor of DNA binding2 is essential for growth cone formation and axon growth and promotes central nervous system axon regeneration. e*Llife*. 5:e20799.
8 Huang ZH, *et al.* 2021. Inhibitor of DNA binding 2 accelerates nerve regeneration after sciatic nerve injury in mice. *Neural Regen Res*. 16(12):2542–2548.
9 Huang Z, *et al.* 2019. Inhibitor of DNA binding 2 promotes axonal growth through upregulation of Neurogenin2. *Exp Neurol*. 320: 112966.
10 Luo W, *et al.* 2021. Recurrent rewiring of the adult hippocampal mossy fiber system by a single transcriptional regulator, Id2. *Proc Natl Acad Sci U S A*. 118(40):e2108239118.
11 Buckmaster PS, Dudek FE. 1999. In vivo intracellular analysis of granule cell axon reorganization in epileptic rats. *J Neurophysiol*. 81(2):712–721.
12 Noebels JL, Avoli M, Rogawski MA, Olsen RW, Delgado-Escueta AV, editors. 2012. *Jasper's basic mechanisms of the epilepsies*. 4th ed. Bethesda (MD): National Center for Biotechnology Information.
13 Luo W, *et al.* 2022. Pcdh11x controls target specification of mossy fiber sprouting. *Front Neurosci*. 16:888362.
14 Egger M, *et al.* 2023. Commissural dentate granule cell projections and their rapid formation in the adult brain. *PNAS Nexus*. 2(4):pgad088.
15 Buckmaster PS. 2012. Mossy fiber sprouting in the dentate gyrus. In: Noebels JL, Avoli M, Rogawski MA, Olsen RW, Delgado-Escueta AV, editors. *Jasper's basic mechanisms of the epilepsies*. 4th ed. Bethesda (MD): National Center for Biotechnology Information (US). p. 1–29.
16 Skinner MK, Rawls A, Wilson-Rawls J, Roalson EH. 2010. Basic helix-loop-helix transcription factor gene family phylogenetics and nomenclature. *Differentiation*. 80(1):1–8.
17 Szklarczyk D, *et al.* 2023. The STRING database in 2023: protein-protein association networks and functional enrichment analyses for any sequenced genome of interest. *Nucleic Acids Res*. 51(D1):D638–D646.
18 Samanta J, Kessler JA. 2004. Interactions between ID and OLIG proteins mediate the inhibitory effects of BMP4 on oligodendroglial differentiation. *Development*. 131(17):4131–4142.
19 Li X, *et al.* 2005. Polycystin-1 and polycystin-2 regulate the cell cycle through the helix-loop-helix inhibitor Id2. *Nat Cell Biol*. 7(12):1202–1212.
20 Lasorella A, Iavarone A. 2006. The protein ENH is a cytoplasmic sequestration factor for Id2 in normal and tumor cells from the nervous system. *Proc Natl Acad Sci U S A*. 103(13):4976–4981.
21 Haenold R, *et al.* 2014. NF-κB controls axonal regeneration and degeneration through cell-specific balance of RelA and p50 in the adult CNS. *J Cell Sci*. 127(Pt 14):3052–3065.
22 Roschger C, Cabrele C. 2017. The Id-protein family in developmental and cancer-associated pathways. *Cell Commun Signal*. 15(1):7.
23 Martin EA, Woodruff D, Rawson RL, Williams ME. 2017. Examining hippocampal mossy fiber synapses by 3D electron microscopy in wildtype and kirrel3 knockout mice. *eNeuro*. 4(3): ENEURO.0088-17.2017.
24 Martin EA, *et al.* 2015. The intellectual disability gene Kirrel3 regulates target-specific mossy fiber synapse development in the hippocampus. e*Llife*. 4:e09395.
25 Maruo T, Mandai K, Takai Y, Mori M. 2016. Activity-dependent alteration of the morphology of a hippocampal giant synapse. *Mol Cell Neurosci*. 71:25–33.
26 Perez Y, Morin F, Beaulieu C, Lacaille JC. 1996. Axonal sprouting of CA1 pyramidal cells in hyperexcitable hippocampal slices of kainate-treated rats. *Eur J Neurosci*. 8(4):736–748.
27 Esclapez M, Hirsch JC, Ben-Ari Y, Bernard C. 1999. Newly formed excitatory pathways provide a substrate for hyperexcitability in experimental temporal lobe epilepsy. *J Comp Neurol*. 408(4): 449–460.
28 Lehmann TN, *et al.* 2000. Alterations of neuronal connectivity in area CA1 of hippocampal slices from temporal lobe epilepsy patients and from pilocarpine-treated epileptic rats. *Epilepsia*. 41(Suppl 6):S190–S194.
29 Smith BN, Dudek FE. 2001. Short- and long-term changes in CA1 network excitability after kainate treatment in rats. *J Neurophysiol*. 85(1):1–9.
30 Marchionni I, Oberoi M, Soltesz I, Alexander A. 2019. Ripple-related firing of identified deep CA1 pyramidal cells in chronic temporal lobe epilepsy in mice. *Epilepsia Open*. 4(2): 254–263.
31 Goebbels S, *et al.* 2006. Genetic targeting of principal neurons in neocortex and hippocampus of NEX-Cre mice. *Genesis*. 44(12): 611–621.
32 Soltesz I, Losonczy A. 2018. CA1 pyramidal cell diversity enabling parallel information processing in the hippocampus. *Nat Neurosci*. 21(4):484–493.
33 Berns DS, DeNardo LA, Pederick DT, Luo L. 2018. Teneurin-3 controls topographic circuit assembly in the hippocampus. *Nature*. 554(7692):328–333.
34 Cembrowski MS, Spruston N. 2019. Heterogeneity within classical cell types is the rule: lessons from hippocampal pyramidal neurons. *Nat Rev Neurosci*. 20(4):193–204.
35 Aaronson DS, Horvath CM. 2002. A road map for those who don't know JAK-STAT. *Science*. 296(5573):1653–1655.
36 Nicolas CS, *et al.* 2013. The role of JAK-STAT signaling within the CNS. *JAKSTAT*. 2(1):e22925.
37 Nallar SC, Kalvakolanu DV. 2014. Interferons, signal transduction pathways, and the central nervous system. *J Interferon Cytokine Res*. 34(8):559–576.
38 Barrat FJ, Crow MK, Ivashkiv LB. 2019. Interferon target-gene expression and epigenomic signatures in health and disease. *Nat Immunol*. 20(12):1574–1583.
39 Ashburner M, *et al.* 2000. Gene ontology: tool for the unification of biology. The Gene Ontology Consortium. *Nat Genet*. 25(1):25–29.
40 Xie Z, *et al.* 2021. Gene set knowledge discovery with Enrichr. *Curr Protoc*. 1(3):e90.

41 Gene Ontology Consortium; Aleksander SA, *et al.* 2023. The gene ontology knowledgebase in 2023. *Genetics*. 224(1):iyad031.
42 Földy C, *et al.* 2016. Single-cell RNAseq reveals cell adhesion molecule profiles in electrophysiologically defined neurons. *Proc Natl Acad Sci U S A*. 113(35):E5222–E5231.
43 de Wit J, Ghosh A. 2016. Specification of synaptic connectivity by cell surface interactions. *Nat Rev Neurosci*. 17(1):22–35.
44 Sanes JR, Zipursky SL. 2020. Synaptic specificity, recognition molecules, and assembly of neural circuits. *Cell*. 181(3):536–556.
45 Südhof TC. 2021. The cell biology of synapse formation. *J Cell Biol*. 220(7):e202103052.
46 Luo L. 2021. Architectures of neuronal circuits. *Science*. 373(6559): eabg7285.
47 Bui AD, *et al.* 2018. Dentate gyrus mossy cells control spontaneous convulsive seizures and spatial memory. *Science*. 359(6377):787–790.
48 Van Den Herrewegen Y, *et al.* 2019. The Barnes maze task reveals specific impairment of spatial learning strategy in the intrahippocampal kainic acid model for temporal lobe epilepsy. *Neurochem Res*. 44(3):600–608.
49 Shuman T, *et al.* 2020. Breakdown of spatial coding and interneuron synchronization in epileptic mice. *Nat Neurosci*. 23(2): 229–238.
50 Deuchars J, Thomson AM. 1996. CA1 pyramid-pyramid connections in rat hippocampus in vitro: dual intracellular recordings with biocytin filling. *Neuroscience*. 74(4):1009–1018.
51 Takács VT, Klausberger T, Somogyi P, Freund TF, Gulyás AI. 2012. Extrinsic and local glutamatergic inputs of the rat hippocampal CA1 area differentially innervate pyramidal cells and interneurons. *Hippocampus*. 22(6):1379–1391.
52 Yang S, *et al.* 2014. Interlamellar CA1 network in the hippocampus. *Proc Natl Acad Sci U S A*. 111(35):12919–12924.
53 Arszovszki A, Borhegyi Z, Klausberger T. 2014. Three axonal projection routes of individual pyramidal cells in the ventral CA1 hippocampus. *Front Neuroanat*. 8:53.
54 Hayashi S, *et al.* 2014. Protocadherin-17 mediates collective axon extension by recruiting actin regulator complexes to interaxonal contacts. *Dev Cell*. 30(6):673–687.
55 Schroeder A, de Wit J. 2018. Leucine-rich repeat-containing synaptic adhesion molecules as organizers of synaptic specificity and diversity. *Exp Mol Med*. 50(4):1–9.
56 Kim J, *et al.* 2022. LRRTM3 regulates activity-dependent synchronization of synapse properties in topographically connected hippocampal neural circuits. *Proc Natl Acad Sci U S A*. 119(3): e2110196119.
57 Sando R, Jiang X, Südhof TC. 2019. Latrophilin GPCRs direct synapse specificity by coincident binding of FLRTs and teneurins. *Science*. 363(6429):eaav7969.
58 Wang S, *et al.* 2024. Alternative splicing of latrophilin-3 controls synapse formation. *Nature*. 626(7997):128–135.
59 Fasen K, Beck H, Elger CE, Lie AA. 2002. Differential regulation of cadherins and catenins during axonal reorganization in the adult rat CNS. *J Neuropathol Exp Neurol*. 61(10):903–913.
60 Yu X, Malenka RC. 2004. Multiple functions for the cadherin/catenin complex during neuronal development. *Neuropharmacology*. 47(5):779–786.
61 Galimberti I, Bednarek E, Donato F, Caroni P. 2010. Epha4 signaling in juveniles establishes topographic specificity of structural plasticity in the hippocampus. *Neuron*. 65(5):627–642.
62 Ranneva SV, Maksimov VF, Korostyshevskaja IM, Lipina TV. 2020. Lack of synaptic protein, calsyntenin-2, impairs morphology of synaptic complexes in mice. *Synapse*. 74(2):e22132.
63 Jiang W, *et al.* 2017. Identification of protein tyrosine phosphatase receptor type O (PTPRO) as a synaptic adhesion molecule that promotes synapse formation. *J Neurosci*. 37(41):9828–9843.
64 Matsuda K, *et al.* 2016. Transsynaptic modulation of kainate receptor functions by C1q-like proteins. *Neuron*. 90(4):752–767.
65 Koumoundourou A, *et al.* 2024. Regulation of hippocampal mossy fiber-CA3 synapse function by a Bcl11b/C1ql2/Nrxn3(25b+) pathway. *eLife*. 12:RP89854.
66 Schultze W, *et al.* 2001. Semaphorin4F interacts with the synapse-associated protein SAP90/PSD-95. *J Neurochem*. 78(3): 482–489.
67 Beesley PW, Herrera-Molina R, Smalla KH, Seidenbecher C. 2014. The neuroplastin adhesion molecules: key regulators of neuronal plasticity and synaptic function. *J Neurochem*. 131(3):268–283.
68 Borreca A, *et al.* 2024. Loss of interleukin 1 signaling causes impairment of microglia- mediated synapse elimination and autistic-like behaviour in mice. *Brain Behav Immun*. 117:493–509.
69 Brennaman LH, Moss ML, Maness PF. 2014. Ephrina/EphA-induced ectodomain shedding of neural cell adhesion molecule regulates growth cone repulsion through ADAM10 metalloprotease. *J Neurochem*. 128(2):267–279.
70 Sullivan CS, *et al.* 2018. Perineuronal net protein neurocan inhibits NCAM/EphA3 repellent signaling in GABAergic interneurons. *Sci Rep*. 8(1):6143.
71 Liu XD, *et al.* 2018. Retrograde regulation of mossy fiber axon targeting and terminal maturation via postsynaptic Lnx1. *J Cell Biol*. 217(11):4007–4024.
72 Beaubien F, Raja R, Kennedy TE, Fournier AE, Cloutier JF. 2016. Slitrk1 is localized to excitatory synapses and promotes their development. *Sci Rep*. 6:27343.
73 Bekirov IH, Nagy V, Svoronos A, Huntley GW, Benson DL. 2008. Cadherin-8 and N-cadherin differentially regulate pre- and postsynaptic development of the hippocampal mossy fiber pathway. *Hippocampus*. 18(4):349–363.
74 Yamagata M, Duan X, Sanes JR. 2018. Cadherins interact with synaptic organizers to promote synaptic differentiation. *Front Mol Neurosci*. 11:142.
75 Asada-Utsugi M, *et al.* 2021. Mice with cleavage-resistant N-cadherin exhibit synapse anomaly in the hippocampus and outperformance in spatial learning tasks. *Mol Brain*. 14(1):23.
76 Duan Y, *et al.* 2014. Semaphorin 5A inhibits synaptogenesis in early postnatal- and adult-born hippocampal dentate granule cells. *eLife*. 3:e04390.
77 Connor SA, *et al.* 2016. Altered cortical dynamics and cognitive function upon haploinsufficiency of the autism-linked excitatory synaptic suppressor MDGA2. *Neuron*. 91(5):1052–1068.
78 Toledo A, *et al.* 2022. MDGAs are fast-diffusing molecules that delay excitatory synapse development by altering neuroligin behavior. *eLife*. 11:e75233.
79 Hsueh YP, Sheng M. 1999. Regulated expression and subcellular localization of syndecan heparan sulfate proteoglycans and the syndecan-binding protein CASK/LIN-2 during rat brain development. *J Neurosci*. 19(17):7415–7425.
80 Sun F, *et al.* 2011. Sustained axon regeneration induced by co-deletion of PTEN and SOCS3. *Nature*. 480(7377):372–375.
81 Pernet V, *et al.* 2013. Misguidance and modulation of axonal regeneration by Stat3 and Rho/ROCK signaling in the transparent optic nerve. *Cell Death Dis*. 4(7):e734–e734.
82 Luo X, *et al.* 2016. Enhanced transcriptional activity and mitochondrial localization of STAT3 co-induce axon regrowth in the adult central nervous system. *Cell Rep*. 15(2):398–410.

83 Duan Q, *et al*. 2024. Stat3 has a different role in axon growth during development than it does in axon regeneration after injury. *Mol Neurobiol*. 61(3):1753–1768.
84 Ivashkiv LB, Donlin LT. 2014. Regulation of type I interferon responses. *Nat Rev Immunol*. 14(1):36–49.
85 Duncan DS, *et al*. 2018. Ccl5 mediates proper wiring of feedforward and lateral inhibition pathways in the inner retina. *Front Neurosci*. 12:702.
86 Xie L, Yin Y, Benowitz L. 2021. Chemokine CCL5 promotes robust optic nerve regeneration and mediates many of the effects of CNTF gene therapy. *Proc Natl Acad Sci U S A*. 118(9): e2017282118.
87 Chodaparambil JV, *et al*. 2014. Molecular functions of the TLE tetramerization domain in Wnt target gene repression. *EMBO J*. 33(7):719–731.
88 Ciani L, Salinas PC. 2005. WNTs in the vertebrate nervous system: from patterning to neuronal connectivity. *Nat Rev Neurosci*. 6(5):351–362.
89 Fuchs E, Cleveland DW. 1998. A structural scaffolding of intermediate filaments in health and disease. *Science*. 279(5350): 514–519.
90 Acsády L, Kamondi A, Sík A, Freund T, Buzsáki G. 1998. GABAergic cells are the major postsynaptic targets of mossy fibers in the rat hippocampus. *J Neurosci*. 18(9):3386–3403.